Recommended Updates to Solubility Controls for Modeling Leaching of Technetium, Uranium, Neptunium, Plutonium, and Iodine from the Residual Waste Layer of Closed Savannah River Site High-Level Waste Tanks

SOL: G-SOW-H-00287

Savannah River Remediation, LLC

February 19, 2021

Signed by Shanthi Dabare, President

Prepared by

IEI
Inspection Experts, Inc.

P:402-802-9983 F:614.386.1999 info@ieinc.net
Corporate: 808 P. St., Suite 318, Lincoln, NE 68508
Business: 9250 Rumsey Rd. Suite 106, Columbia MD 21045

This report was prepared by Panoramic Environmental Consulting, LLC under Professional Services Subcontract Agreement 2024 with Inspection Experts, Inc. and funded by Savannah River Remediation, LLC.

Disclaimer

Table of Contents

Executive Summary 4
Introduction 6
Background 6
Relation of Experimental Results to Modeling Results 7
Interpretation of SRNL Experimental Results 8
Updated Thermodynamics 8
Activity-Activity Diagrams 9
Mass Available for Leaching 11
Coprecipitation 11
Technetium 12
Uranium 15
Neptunium 21
Plutonium 23
Iodine 25
Conclusion 27
References 29
Appendix 1: Results from residual waste leaching experiments done by King and Hobbs (2016) and King (2018) 32

List of Figures

Figure 1: Solubilities of gibbsite (green) and hematite (orange) at Eh=0.24 V; calculated using the "themochimie_GWB_electron.v10a.dat" database. 12

Figure 2: Comparison of Eh-pH measurements in SRNL waste leaching experiments with the stability field for TcO_2(am,hyd,aged) calculated with The Geochemist's Workbench® using a Tc activity of 10^{-7}. . 13

Figure 3: Eh-pH values of samples in SRNL experiments relative to the stability of UO_2(am,hyd) at a uranium activity of 10^{-6} M. 16

Figure 4: Calculated diagram of uranium concentration vs. pH showing where average sample measurements for the Reduced Region II and Oxidized Region II plot relative to stability fields of five potential solubility controlling minerals. 17

Figure 5: Calculated diagram of uranium concentration vs. pH showing where average sample measurements for Oxidized Region III plot relative to stability fields of four potential solubility controlling mineral at aqueous concentrations of Na^+, Ca^{+2}, and $Si(OH)_4$ approximated for addition of cementitious materials. 18

Figure 6: Calculated diagram of uranium concentration vs. pH showing where average sample measurements for the Oxidized Region III experiment plot relative to stability fields of four potential solubility controlling mineral. 19

Figure 7: Hypothetical stability field for a uranophane-like Np(V) phase calculated using a logKsp derived by Murphy and Grambow (2008); arrows indicate concentrations below detection limits. 22

Figure 8: Stability field of crystalline $NpO_{2(cr)}$ compared to other neptunium phases; arrows indicate concentrations below detection limits. 23

Figure 9: Stability field of a Pu(IV) in equilibrium with atmospheric CO_2, calculated using thermodynamic data from Yamaguchi et al (1994). 24

Figure 10: Plutonium leachability data from SRNL experiments compared to calculated solubility of PuO2(am,hyd) with no colloidal particles (dashed lines show thermodynamic uncertainty given by Grenthe et al. (2020)) and with colloidal particles after Neck et al. (2007a). 25

Figure 11: Eh-pH diagram for silver-iodine system, showing stability fields for AgI(s) and Ag metal and Eh-pH measurements from Tank 12H experiments. 26

Figure 12: Eh-pH diagram for the mercury-iodine system showing stability fields for mercury iodide phases, mercury metal and Eh-pH measurements from Tank 12H experiments. 27

List of Tables

Table 1: Composition of pore fluids in grout degradation regions calculated by Denham and Millings (2013)..... 6

Table 2: LogK˚ values of dissociation and dissolution reactions of aqueous species (blue) and solid phases (black) that were significantly different between the thermodynamic data used in Denham and Millings (2012) and the updated NEA data..... 9

Table 3: Comparison of calculated solubilities from Denham and Millings (2012) to those calculated using the new NEA thermodynamic data. 10

Table 4: Estimated mass of radionuclides in the residual waste samples used in the SRNL leaching experiments and the maximum fraction leached during an experiment..... 11

Table 5:Average Tc-99 concentrations (M) in three Tank 12H experiments that reconditioned samples with fresh fluid during the experiment. 14

Table 6: Calculated solubilities for technetium phases selected to control leachability..... 15

Table 7: Minerals and their formulas used to explain SRNL experimental results. 16

Table 8: Solubilities of becquerelite and uranophane calculated for Oxidizing Region II and Oxidizing Region III using updated NEA thermodynamic data and fluid compositions assumed in Denham and Millings (2012)..... 21

Executive Summary

The objective of this report is to relate waste leaching experiments by the Savannah River National Laboratory (SRNL) to performance assessment modeling of release of several radionuclides from residual waste in closed high-level waste tanks. SRNL leached residual waste from Tanks 18F and 12H with solutions simulating the modeled evolution of pore fluids in residual waste layers of closed tanks through various stages of grout degradation. Tc-99, uranium isotopes, Np-237, plutonium isotopes, and I-129 were analyzed in the leachate multiple times over 90 days.

A fundamental limitation of all experiments using actual residual waste conducted to inform modeling of long-term radionuclide release from closed waste tanks is that the nature of the residual waste will change significantly after closure of the tanks and over the time periods simulated by performance assessment modeling. Some mechanisms that control release of radionuclides from residual waste will change, while others may not. Nevertheless, the SRNL experiments are a starting point for understanding mechanisms that control leachability of radionuclides from residual waste in closed waste tanks. Interpretation of the experimental results in this report posits specific mechanisms, where possible, that can explain radionuclide leaching results. Final recommendations on updating modeled release of the pertinent radionuclides includes qualitative assessment of whether the suggested mechanisms are likely to change after tank closure.

Specific phases are identified in this report with solubilities that account for total uranium and plutonium concentrations in the leachate of the experiments. In contrast, I-129 concentrations in leachate were below detection limits, as were most Np-237 concentrations. While specific controls on Np-237 and I-129 leachability cannot be recommended, known plausible mechanisms for constraints on their leachability exist and recommendations are made for modeling their release from residual waste. Possible mechanisms to explain low Tc-99 concentrations in leachate are discussed, including limited mass of Tc-99 available for leaching. Plausibility of other mechanisms that limitTc-99 release in oxidizing conditions is uncertain, particularly whether the mechanisms could persist in closed tanks for long periods of time. Despite the low Tc-99 concentrations in experimental leachate, it is recommended that no solubility controls on Tc-99 be used to model release from residual waste.

The table on the following page summarizes the results of this review. The “2012” recommendations are from Denham and Millings (2012), informed by only minimal experimental data. The updated recommendations are based on the SRNL experiments. The recommendations for plutonium have not changed from the 2012 recommendations. The only change for technetium is to use the more general hydrated amorphous phase $TcO_{2(am,hyd)}$ under reducing conditions, rather than the phase with a specific hydration state of $TcO_2 \cdot 1.6H_2O$. Recommendations on leachability controls for uranium, neptunium, and iodine have changed significantly since 2012. Solubilities and activity-activity diagrams calculated in this report will have to be recalculated if future grout degradation modeling predicts pore fluid compositions that are significantly different than predicted in previous modeling.

		Technetium	Uranium	Neptunium	Plutonium	Iodine
Red.Reg.II	2012[1]	$TcO_2 \cdot 1.6H_2O$	$UO_{2(am,hyd)}$	$NpO_{2(am,hyd)}$	$PuO_{2(am,hyd)}$	SRNL Detection Limits[4]
	Updated	$TcO_{2(am,hyd,aged)}$	$UO_{2(am,hyd)}$	SRNL Detection Limits[4]	$PuO_{2(am,hyd)}$	SRNL Detection Limits[4]
Ox.Reg.II	2012[1]	No Control	$UO_3 \cdot 2H_2O$	$NpO_{2(am,hyd)}$	$PuO_{2(am,hyd)}$	SRNL Detection Limits[4]
	Updated	No Control	Becquerelite[2] Uranophane[3]	SRNL Detection Limits[4]	$PuO_{2(am,hyd)}$	SRNL Detection Limits[4]
Ox.Reg.III	2012[1]	No Control	$UO_3 \cdot 2H_2O$	$NpO_{2(am,hyd)}$	$PuO_{2(am,hyd)}$	SRNL Detection Limits[4]
	Updated	No Control	Becquerelite[2] Uranophane[3]	Avg. SRNL Test Values	$PuO_{2(am,hyd)}$	SRNL Detection Limits[4]

[1] – Denham and Millings (2012) recommendation

[2] – as pessimistic case; Becquerelite = $CaU_6O_{19} \cdot 11H_2O_{(cr)}$ in NEA thermodynamic database

[3] – as optimistic case; Uranophane = $Ca(UO_2)_2(SiO_3OH)_2 \cdot 5H_2O_{(cr)}$ in NEA thermodynamic database

[4] – highest detection limit with caveat that control is based on limited data

Introduction

The purpose of this document is to provide guidance for updating solubilities of key radionuclides used in performance assessment (PA) of closed Savannah River Site (SRS) high level waste tanks. New experimental data on leaching of residual waste from two tanks has been collected and new thermodynamic data has been published since the last time solubilities were calculated. This document uses these new data to assess the choices of solubility controlling phases and, where warranted, provides new calculated solubilities for technetium, uranium, neptunium, plutonium, and iodine for use in PA modeling.

Background

Closure of high-level waste tanks at SRS involves emptying the tanks and removing as much of the residual waste at the bottom of the tanks as possible. The tanks are then filled with low permeability grout that is a barrier to future water infiltration and leaching of radionuclides from the residual waste. PA modeling of tank closure uses numerical models that have limited reactive transport capabilities. They cannot directly account for variations in radionuclide leachability as pore fluids in the residual waste evolve in response to chemical degradation of the tank-filling grout. Denham and Millings (2012) developed a reaction path model of SRS tank grout degradation in which each pore volume of infiltrating water was assumed to react to equilibrium with cementitious minerals, followed by replacement by another pore volume of infiltration. The results of the reaction path model were three distinct phases of grout evolution with durations in units of pore volumes. Each phase had a characteristic pore fluid composition (**Table 1**). They then calculated key radionuclide solubilities in each pore fluid composition to control radionuclide leachability from the residual waste layer. The predictive models converted the pore volumes of infiltration to time, and thus were able to vary leachability with time. Denham and Millings (2012) developed the solubility controls of radionuclides with sparse empirical data on actual radionuclide-bearing solid phases in the residual waste or the radionuclide leachability.

Table 1: Composition of pore fluids in grout degradation regions calculated by Denham and Millings (2013).

Component	Reduced Region II	Oxidized Region II	Oxidized Region III
pH	11.1	11.1	9.2
Eh (V)	-0.47	0.24	0.29
Calcium (M/L)	4.0E-3	4.0E-3	6.6E-5
Dissolved Inorganic Carbon (M/L)	6.7E-7	6.7E-7	7.5E-5
Sulfate (M/L)	1E-5	1E-5	1.0E-5
Sodium (M/L	1E-3	1E-3	1.0E-3
Chloride (M/L	1E-3	1E-3	1.0E-3
Oxalate (M/L)	4.1E-6	4.1E-6	4.4E-5

King and Hobbs (2016) and King (2018) leached actual residual waste samples with fluids that approximated the compositions of the three grout degradation regions to provide empirical data to inform updates to the modeling of radionuclide leaching from closed tanks. They analyzed the leachate several times during the experiments for concentrations of technetium-99 (Tc-99), neptunium-237 (Np-237), iodine-129 (I-129), uranium isotopes and plutonium isotopes, as well as Eh and pH. The summary results appear here in Appendix 1, with isotopes of uranium and plutonium summed to total molar concentrations. King and Hobbs (2016) used residual waste samples from Tank 18F. This tank was

cleaned mechanically using methods that involved large quantities of water, but no aggressive leachant. King (2018) used samples from Tank 12H that was cleaned mechanically and chemically using oxalic acid. The experimental details are available in the reports and are summarized in Layton (2018a). Hence, they are not discussed here except when specific details are invoked in the interpretation of the results. Hereafter, the term "SRNL experiments" is used to refer to both sets of experiments and the report citation is used when referring to a specific set of experiments.

Relation of Experimental Results to Modeling Results

The interpretation of the SRNL experiments attempts to bridge the gap between experiments and modeling. Measurements of radionuclide leaching from actual residual waste samples are invaluable, yet they cannot be used directly in predictive models because the nature of the samples used is different from the residual waste that will be leached far into the future.

The samples used in the SRNL experiments were on the order of years old and relatively unaltered from their state in the tanks except for an initial washing with representative pore fluid simulants prior to the experiments. In contrast, leaching of the residual waste layer will not begin until the tank is breached and pore fluids begin flowing through the layer. That may not occur for a period of time on the order of 100s to 1000s of years. At that time, the residual waste layer will be exposed to chemically reducing pore fluids with high pH (12-13) and high concentrations of alkali metals, calcium, and silica. Some changes in mineralogy and crystallinity of the waste layer matrix and radionuclide-bearing phases are inevitable, but the exact changes are unknown.

Additional changes in mineralogy may occur in response to exposure to the leachant. These are much more likely to occur over the timescales considered for PA modeling than during the 90-day experiment. Once leaching of the residual waste layer begins, the alkali metals will rapidly flush from the layer leaving it exposed to reducing, moderately high pH (10-11) fluid with moderately high calcium and silica concentrations (Reducing Region II) for 1000s of years. The residual waste layer will be exposed to the fluid composition associated with the successive regions of grout degradation for thousands of years each. Thus, the mineralogy throughout the experiments remains the same, whereas the mineralogy of the actual residual waste layer is likely to evolve as the composition of pore fluids change.

Interpretation of the experimental data, within the framework of the residual waste layer conceptual model, requires identifying solid phases that have solubilities that can explain the experimental results. The next step is assessing whether these phases are likely to occur under the conditions of a closed tank. Identification of phases that can explain the results does not mean that these phases have been identified in the samples, or even exist in the samples. Nevertheless, it provides some level of confidence in the conceptual model and the choice of solubility controls. It is also noteworthy that the experimental results often provide a worst-case scenario because as the waste ages in the closed tanks most radionuclides will not become more soluble. Poorly crystalline phases will only become more crystalline and less soluble and moderately soluble minerals are likely to react with available constituents to become less soluble.

Another important aspect of interpreting the experimental results is understanding the uncertainties inherent in assigning solubilities for radionuclides. There are uncertainties in the thermodynamic data required for calculating solubilities. Solubilities can only be calculated for pure phases, but the purity of phases in a system as chemically complex as a high-level waste tank or a closed waste tank is uncertain.

There is uncertainty in assigning solubilities in systems that are not perfectly and completely characterized – a standard that no experiment meets. If solubility controlling variables are unknown or poorly constrained, calculated solubilities can vary by over an order of magnitude. The variations in solubilities of technetium, uranium, neptunium, and plutonium with the controlling variables pH, Eh, and carbonate concentration at conditions pertinent to grouted tanks are explored in pages 43-78 of Denham and Millings (2012).

Interpretation of SRNL Experimental Results

Updated Thermodynamics

Denham and Millings (2012) calculated solubility values for solid phases of uranium, neptunium, plutonium, and technetium from free energy data for the pertinent solid phases and aqueous species that were downloaded from the Nuclear Energy Agency (NEA) Data Bank in 2011. The NEA is the agency within the Organisation for Economic Co-operation and Development (OECD) responsible for developing information and guidance related to nuclear energy and waste management. The OECD is composed of 37 countries and brings together experts from member countries to cooperate on projects related to economic development. Over the past three decades the NEA has assembled teams of experts to review all available published studies on thermochemistry of several radioactive elements, as well as other elements important to nuclear energy issues, to produce authoritative compilations of thermochemical data. The data are available in published volumes and digitally at the NEA Thermochemical Database Project homepage (https://www.oecd-nea.org/jcms/pl_22166/thermochemical-database-tdb-project). The thermochemical data used in Denham and Millings (2012) were from NEA sources up through 2003 (Grenthe et al., 1992; Rard et al., 1999; Lemire et al., 2001; Guillaumont et al., 1992). The NEA released an update of thermochemical data for uranium, neptunium, americium, plutonium, and technetium in 2020 that includes reviews of published studies through 2017 (Grenthe et al., 2020).

To compare the results of the experiments by King and Hobbs (2016) and King (2018) on leaching of uranium, neptunium, plutonium, and technetium from residual tank waste to calculated solubility values, the calculated values have been updated based on the most recent NEA data. The data was downloaded from the NEA website as a complete dataset in PHRREQC format, ready for geochemical modeling. The PHREEQC database was converted to The Geochemist's Workbench® format. **Table 2** (following page) lists the aqueous species and solid phases of uranium, neptunium, plutonium, and technetium for which the logK˚ values of the dissociation and dissolution reactions are significantly different in the updated NEA thermodynamic data than shown in Appendix 2 of Denham and Millings (2012). Significant is arbitrarily defined here as a difference in logK˚ of reaction that results in a 10% difference in values of K˚ for the reaction. There were significant changes in the logK˚ values for the dissolution reactions of solid phases of uranium and plutonium that were used to control solubility in Denham and Millings (2012). The changes in the aqueous species are not significant to solubility calculations for any of the radionuclides in Reduced Region II, Oxidized Region II, and Oxidized Region III.

Table 2: LogK˚ values of dissociation and dissolution reactions of aqueous species (blue) and solid phases (black) that were significantly different between the thermodynamic data used in Denham and Millings (2012) and the updated NEA data.

Aqueous Species/Solid Phase	Denham and Millings (2012)	Grenthe (2020)
$UO_{2(am,hyd)}$	1.660	1.505
$UO_3 \cdot 2H_2O_{(cr)}$	4.811	5.350
$NpO_2(CO_3)_{(aq)}$	-9.320	-9.860
$NpO_2(CO_3)_3^{-4}$	-19.371	-19.900
$NpO_2CO_{3(s)}$	-14.597	-14.830
$NpO_2OH_{(am)}$	4.700	5.300
$PuOH^{+2}$	6.900	6.180
$PuO_2CO_3^-$	-5.120	-5.030
$PuO_2(CO_3)_3^{-5}$	-5.030	-5.610
$PuO_{2(am,hyd)}$	-1.990	-2.325
$PuO_2CO_{3(s)}$	-14.650	-14.820

Solubilities of pertinent phases of uranium, neptunium, plutonium, and technetium were calculated for Reduced Region II, Oxidized Region II, and Oxidized Region III using the updated thermodynamic data. **Table 3** (following page) shows the calculated solubilities using the updated NEA thermodynamic data compared to those in Denham and Millings (2012). The solubilities of uranium using the updated data decreased slightly in Reduced Region II and increased significantly in the oxidized regions, consistent with the logK˚ values in **Table 1**. The solubilities of neptunium and plutonium do not change significantly. The solubility of technetium decreases in Reduced Region II and there is still no solubility control in the oxidized regions. It should be noted that the phase controlling solubility of technetium under reducing conditions was changed from $TcO_2 \cdot 1.6H_2O$, used in Denham and Millings (2012), to TcO_2(am, hyd, aged) using the new NEA data. Grenthe et al. (2020) discuss the evidence that the degree of hydration of amorphous TcO_2 decreases over time, a matter of a few days, and the fact that the solubility is not influenced substantially by the degree of hydration. Thus, they suggest using TcO_2(am, hyd, fresh) for freshly precipitated TcO_2 and TcO_2(am, hyd, aged) for older TcO_2. Review of the solubility calculations shows that there are no aqueous complexes among those controlling solubility in the new NEA data that were not in the database used in the calculations of Denham and Millings (2012).

Activity-Activity Diagrams

The interpretation of SRNL experimental results uses activity-activity diagrams to illustrate solubility and other controls on leachability of radionuclides. All diagrams were calculated using The Geochemist's Workbench®, Release 15 (Bethke et al., 2021). In most cases, the diagrams were calculated using the latest NEA thermodynamic data, unless otherwise stated. In construction of the diagrams, it is assumed that conditions approach ideal and activity coefficients equal 1, so that molality equals activity. The diagrams are used because they allow examination of chemical controls on leachability of radionuclides over a wide range of conditions, as well as illustrate the sensitivity of different solubility controlling phases to pH and other parameters.

Table 3: Comparison of calculated solubilities from Denham and Millings (2012) to those calculated using the new NEA thermodynamic data.

Uranium			
Degree of Grout Evolution	**Original/Updated**	**Solubility (mol/liter)**	**Phase**
Reduced Region II	Denham and Millings (2012)	5E-09	$UO_{2(am,hyd)}$
	Updated	3E-09	$UO_{2(am,hyd)}$
Oxidized Region II	Denham and Millings (2012)	5E-05	$UO_3 \cdot 2H2O$
	Updated	2E-04[a]	$UO_3 \cdot 2H2O$
Oxidized Region III	Denham and Millings (2012)	4E-06	$UO_3 \cdot 2H2O$
	Updated	4E-05[a]	$UO_3 \cdot 2H2O$
Neptunium			
Degree of Grout Evolution	**Original/Updated**	**Solubility (mol/liter)**	**Phase**
Reduced Region II	Denham and Millings (2012)	1E-09	$NpO_{2(am,hyd)}$
	Updated	1E-09	$NpO_{2(am,hyd)}$
Oxidized Region II	Denham and Millings (2012)	3E-07	$NpO_{2(am,hyd)}$
	Updated	3E-07[b]	$NpO_{2(am,hyd)}$
Oxidized Region III	Denham and Millings (2012)	2E-06	$NpO_{2(am,hyd)}$
	Updated	2E-06	$NpO_{2(am,hyd)}$
Plutonium			
Degree of Grout Evolution	**Original/Updated**	**Solubility (mol/liter)**	**Phase**
Reduced Region II	Denham and Millings (2012)	3E-11	$PuO_{2(am,hyd)}$
	Updated	2E-11	$PuO_{2(am,hyd)}$
Oxidized Region II	Denham and Millings (2012)	3E-11	$PuO_{2(am,hyd)}$
	Updated	2E-11	$PuO_{2(am,hyd)}$
Oxidized Region III	Denham and Millings (2012)	3E-11	$PuO_{2(am,hyd)}$
	Updated	2E-11	$PuO_{2(am,hyd)}$
Technetium			
Degree of Grout Evolution	**Original/Updated**	**Solubility (mol/liter)**	**Phase**
Reduced Region II	Denham and Millings (2012)	1E-08	$TcO_2 \cdot 1.6H_2O$
	Updated	5E-09	$TcO_{2(am,hyd,aged)}$
Oxidized Region II	Denham and Millings (2012)	No Limit	----
	Updated	No Limit	----
Oxidized Region III	Denham and Millings (2012)	No Limit	----
	Updated	No Limit	----

a—Supersaturated with $CaU_6O_{19} \cdot 11H_2O$

b—Supersaturated with $Ca_{0.5}NpO_2 \cdot 1.3H_2O$

Mass Available for Leaching

To assess controls on leachability of a radionuclide, it is important to establish that the control on concentrations in the experiments was not simply a lack of the radionuclide mass in the samples of residual waste. A radionuclide may be 100% leachable, but a low concentration in the solid samples will result in a low concentration in the leachate. **Table 4** shows the estimated average mass of Tc-99, U-238, Np-237, Pu-239, and I-129 in samples used for the Tank 18F and Tank 12H experiments. The masses were calculated from the analyses of residual waste prior to leaching provided in King and Hobbs (2016) and King (2018). The fraction leached represents the fraction of the radionuclide mass in the solid that was dissolved into the leachate, based on the highest concentration observed during the leaching experiments. The masses of radionuclides in leachate are generally low relative to the masses in the solids and the fractions leached are low, suggesting that mass limitations are not controlling leachate concentrations. The high fractions leached of U-238 in Tank 18F experiments and Tc-99 are notable and discussed below.

Table 4: Estimated mass of radionuclides in the residual waste samples used in the SRNL leaching experiments and the maximum fraction leached during an experiment.

Radionuclide	Moles per Experiment		Fraction Leached	
	Tank 18F	Tank 12H	Tank 18F	Tank 12H
Tc-99	1.6E-7	1.8E-8	1.7E-2	1.4E-1
U-238	7.3E-4	9.8E-5	9.2E-2	5.1E-3
Np-237	2.1E-7	1.3E-6	3.9E-3	1.9E-4
Pu-239	4.6E-6	1.9E-6	3.9E-4	2.6E-5
I-129	--	1.9E-6	--	1.3E-3

Coprecipitation

Solubility is not controlled by coprecipitation with iron or aluminum phases for any of the radionuclides analyzed in the SRNL leaching experiments. Hematite (Fe_2O_3) and gibbsite ($Al(OH)_3$) are dominant phases identified in the Tank 18F samples (King and Hobbs, 2016) and hematite was a dominant phase in Tank 6F residual waste (Poirier et al., 2009). Both hematite and gibbsite are approximately 2 orders of magnitude less soluble at pH=9 than pH=11 (**Figure 1**). The basis for calculating apparent solubilities of radionuclides precipitated in a bulk waste phase is that the radionuclide is released from the bulk phase at a concentration that is the product of the bulk phase solubility and the molar ratio of the radionuclide to the major cation in the bulk phase. Thus, the apparent solubility of a radionuclide coprecipitated in either hematite (or any other iron mineral) or gibbsite should be approximately 2 orders of magnitude lower in Oxidized Region III than in Oxidized Region II. This was not observed for any radionuclide in either the Tank 18F or Tank 12H experiments. In addition, the solubilities of the radionuclides analyzed in the SRNL experiments are generally too high to reflect coprecipitation with an iron phase.

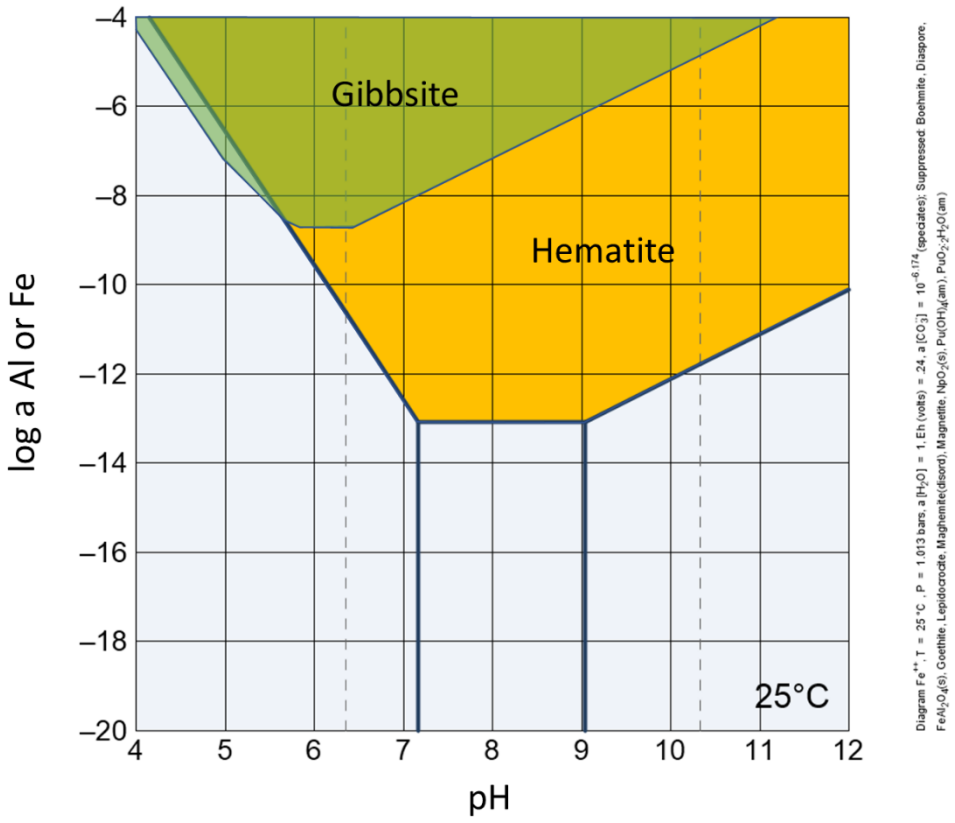

Figure 1: Solubilities of gibbsite (green) and hematite (orange) at Eh=0.24 V; calculated using the "themochimie_GWB_electron.v10a.dat" database.

Technetium

The concentrations of Tc-99 in leachate from the SRNL experiments were consistently between 10^{-8} and 10^{-9} M (moles/liter) for both Tank 18F and Tank 12H solids. Only 8 of 50 measured Tc-99 concentrations in experiments using Tank 12H solids were outside the range of 10^{-8} to 10^{-9} M. In Tank 18F experiments, 15 of 39 Tc-99 concentrations were outside that range. All Tc-99 concentrations that were outside the range of 10^{-8} to 10^{-9} M were lower than 10^{-9} M, in both Tank 12H and Tank 18F experiments.

Tc-99 concentrations between 10^{-8} and 10^{-9} M are lower than expected for the oxidized regions of grout degradation (no solubility control) and approximately equal to the concentration expected for Reduced Region II (5E-9 M). Yet, **Figure 2** (following page) shows that the Eh values measured in the experiments, even most of the Reducing Region II experiments, never approached conditions required to reduce TcO_4^- to amorphous TcO_2. Moreover, **Table 4** shows that the fraction of total mass of Tc-99 leached from the solids used in the experiments was 0.017 for Tank 18F and 0.14 for Tanks 12H. This means that despite the relatively low concentrations of Tc-99 in the leachate, a relatively high fraction of Tc-99 was leached from the solids. Interestingly, a high fraction of the Tc-99 was leached from the Tank 12H solids even though this tank was chemically cleaned (Layton, 2018a) and the samples were washed prior to beginning the experiments. The assumption in Denham and Millings (2012) was that chemical cleaning of a tank would remove the easily leachable Tc-99 and the remainder would be coprecipitated.

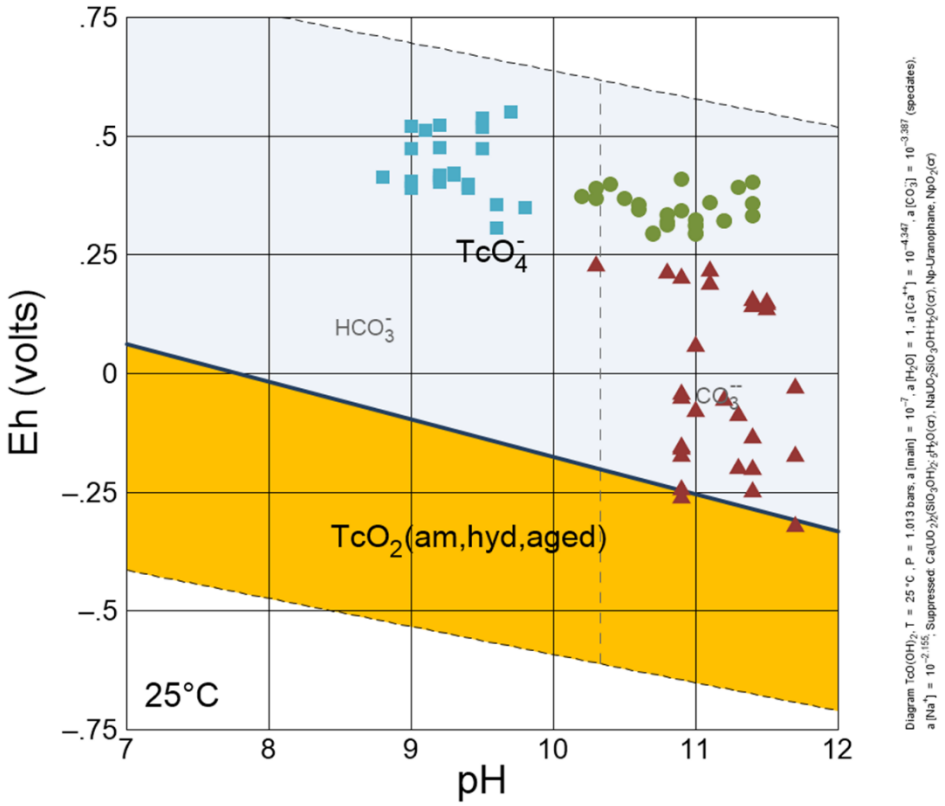

Figure 2: Comparison of Eh-pH measurements in SRNL waste leaching experiments with the stability field for TcO_2(am,hyd,aged) calculated with The Geochemist's Workbench® using a Tc activity of 10^{-7}.

There are two plausible mechanisms to explain the behavior of Tc-99 in the SRNL experiments. One is that leachability of Tc-99 was physically controlled by limited access of experimental solutions to TcO_2 particles and Tc-99 that was exposed to solutions was leached with little to no solubility control. The other is that ferrous iron in the solid matrix mediated reduction of Tc-99 to amorphous TcO_2 at the surface particle surfaces.

Grenthe et al. (2020) discuss that amorphous TcO_2 often precipitates as colloidal particles with diameters of 10s of nanometers. Incorporation of these particles into iron oxide matrix is a possible mechanism of coprecipitation of Tc-99 and Denham and Millings (2012) assumed that the apparent solubility would be the product of the ratio of Tc/Fe in the iron oxide and its solubility. This results in apparent solubilities for coprecipitated Tc-99 that are less than 10^{-13} M. Yet, in an experiment where waste samples are disaggregated and agitated in a slurry, TcO_2 exposed at the microporous surface of particles would be subject to leaching at the solubility of amorphous TcO_2 – low in reducing conditions, high in oxidizing conditions.

Under the Eh-pH conditions achieved in the SRNL experiments, TcO_2 at the surface of waste particles would be expected to dissolve without solubility controls, limited only by the rate of dissolution. There is some evidence of this in the experiments that were interrupted to wash the samples. This was done in the Reducing Region II experiments to mimic the conceptual model and in the Oxidized Region III-B

experiment in which the solids were inadvertently washed during the test because of a broken vessel. In these cases, the fluid was replaced with fresh fluid for the second portion of the experiment. **Table 5** shows the average Tc-99 concentrations from the first and second portion of the Tank 12H experiments (Tank 18F experiments are not shown because most of the Tc-99 concentrations were below detection). In all three experiments, the Tc-99 concentrations are lower in the second portion of the experiment. One explanation is that the dissolution of Tc-99 was only constrained by kinetics, not solubility, and most of theTc-99 in contact with solution was dissolved in the first portion. In the second portion there was less mass to dissolve, and thus, lower concentrations in solution.

Table 5: Average Tc-99 concentrations (M) in three Tank 12H experiments that reconditioned samples with fresh fluid during the experiment.

Experiment	Average Tc-99 (M) 1st Stage	Average Tc-99 (M) 2nd Stage
RRII-CC	3E-9	≤6E-10
RRII-CFS	1E-8	2E-9
ORII-B	6E-9	≤2E-10

There is a body of work that demonstrates the association of technetium with iron oxides. Zachara et al. (2007) and Peretyazhko et al. (2009) demonstrated that ferrous iron can rapidly oxidize TcO_4^- to TcO_2 at the surface of iron minerals under anoxic conditions. At the end of the reduction experiment in the anoxic environment the technetium concentrations were approximately the same as amorphous TcO_2 under reducing conditions. Zachara et al. (2007) found that the re-oxidation rate of Tc(IV) in the iron precipitate was slower than oxidation of amorphous TcO_2. Meena and Arai (2017) and Boglaienko and Levitskaia (2019) review a number of other studies in which Tc(IV) is incorporated into iron oxides by addition of ferrous iron in dissolved and mineral phases. Fredrickson et al. (2009) introduced TcO_4^- into two different bioreduced sediments, demonstrated the reduction to Tc(IV), and then observed the rate of re-oxidation of technetium when exposed to air. The rate of re-oxidation was rapid in one sediment and slow in the other. Though the reoxidation rate was reduced, the technetium concentration exceeded 10^{-6} M in less than 10 days. They found that the reoxidation rate was slow because Tc(IV) was bound in minerals, such as phyllosilicates, into which oxygen diffusion was limited. Szecsody et al. (2014) observed rapid reduction of TcO_4^- in anaerobic sediment and re-oxidation rates that varied with the mineralogy of the sediment. Rates of re-oxidation were slow when Tc(IV) was occluded by mineral precipitation, trapped in immobile porosity, or was in sediments containing sulfide. Nevertheless, concentrations of technetium in the slowly oxidizing systems were on the order of 10^{-5} M after 450 hours.

Thus, technetium can be reduced under oxygen-free conditions by ferrous iron at the surface of iron oxide minerals. In the studies cited above, re-oxidation was hindered by incorporation of Tc(IV) into mineral matrices, occlusion by precipitating iron oxides, or other mechanisms that limit the exposure of Tc(IV) to oxygen. However, though the rate of re-oxidation is decreased by these mechanisms, the solubility of technetium was not limited to 10^{-8} to 10^{-9} M. Solubility constraints under oxidizing conditions only apply to truly coprecipitated technetium and the constraint is the solubility of the iron phase. Nevertheless, it is possible that adsorbed ferrous iron or magnetite at the surface of micropores in residual waste particles in the SRNL experiments could have limited diffusion of oxygen and maintained conditions in which amorphous TcO_2 was stable within the pores. This mechanism of mediating the oxidation-reduction of technetium is transitory, but may have constrained technetium

concentrations in the experimental solutions to the solubility of TcO_2 under reducing conditions. A continual supply of dissolved oxygen to the system, by bubbling air in the experiments or by infiltrating pore fluids in a closed tank, would eventually deplete the supply of ferrous iron in the micropores and leaching of technetium in contact with pore fluids will be controlled by kinetics, not solubility.

Another transitory mechanism for release of Tc-99 in the leaching experiments that might explain the low leachate concentrations and high removal percentage of Tc-99 in the leaching experiments is coprecipitation in a moderately soluble salt. Poirier et al. (2009) found nickel oxalate hydrate in residual waste from Tank 6F and Layton (2018b) discussed the possibility of other metal oxalates precipitating during tank cleaning with oxalic acid. An objective of cleaning with oxalic acid is to remove as much of the recalcitrant bulk solids, such as iron oxides, and the radionuclide that are bound within them. Small amounts of Tc-99 could have coprecipitated with metal oxalates as the Tc-99 was released from dissolving iron oxides or other recalcitrant phases. Tc-99 would have been re-dissolved during the leaching experiments at a concentration that was a function of the oxalate phase solubility and the concentration of coprecipitated Tc-99.

These are all hypothetical mechanisms to explain low concentrations of Tc-99 in the leachate of the SRNL experiments under oxidizing conditions. None would provide a long-term source of low solubility Tc-99 in a closed tank under oxidizing conditions.

Modeling of tank closure performance should reflect mechanisms of Tc-99 release from residual waste that are known to operate over long timeframes. Solubility controls exerted by dissolution of discrete aged TcO_2 particles is a long-term processes and updated values for these are presented in **Table 6**. The values are based on the most recent NEA thermodynamic data. The value of 5E-9 M for solubility of TcO_2(am,hyd,aged) is nearly identical to the value of 1E-8 M for $TcO_2 \cdot 1.6H_2O$ used by Denham and Millings (2012).

Table 6: Calculated solubilities for technetium phases selected to control leachability.

Pertinent Solubility Controlling Mineral	Reducing Region II	Oxidizing Region II	Oxidizing Region III
TcO_2(am,hyd,aged)	5E-9	No Solubility Control	No Solubility Control

Denham and Millings (2012) assumed that minimal coprecipitated Tc-99 would be lost from iron minerals during phase changes from hematite to magnetite to maghemite. Marshall et al. (2014) provided experimental evidence related to this assumption. They produced magnetite with coprecipitated technetium and oxidized the magnetite to maghemite. During the oxidation approximately 30% of the technetium originally in the magnetite was lost to solution and 70% retained by the maghemite.

Uranium

The SRNL experimental results for uranium leaching from residual waste reflect the complicated chemistry of uranium and how the varied history of samples affects uranium leaching. It was assumed in Denham and Millings (2012) that uranium would exist as low solubility U(IV) in Reducing Region II. The solubility controlling phase selected was UO_2(am,hyd). As **Figure 3** illustrates, only a few samples in the Reducing Region II approached conditions necessary for reduction of U(VI) to U(IV) and precipitation of UO2(am,hyd). Thus, this analysis examines U(VI) phases that may explain the experimental results.

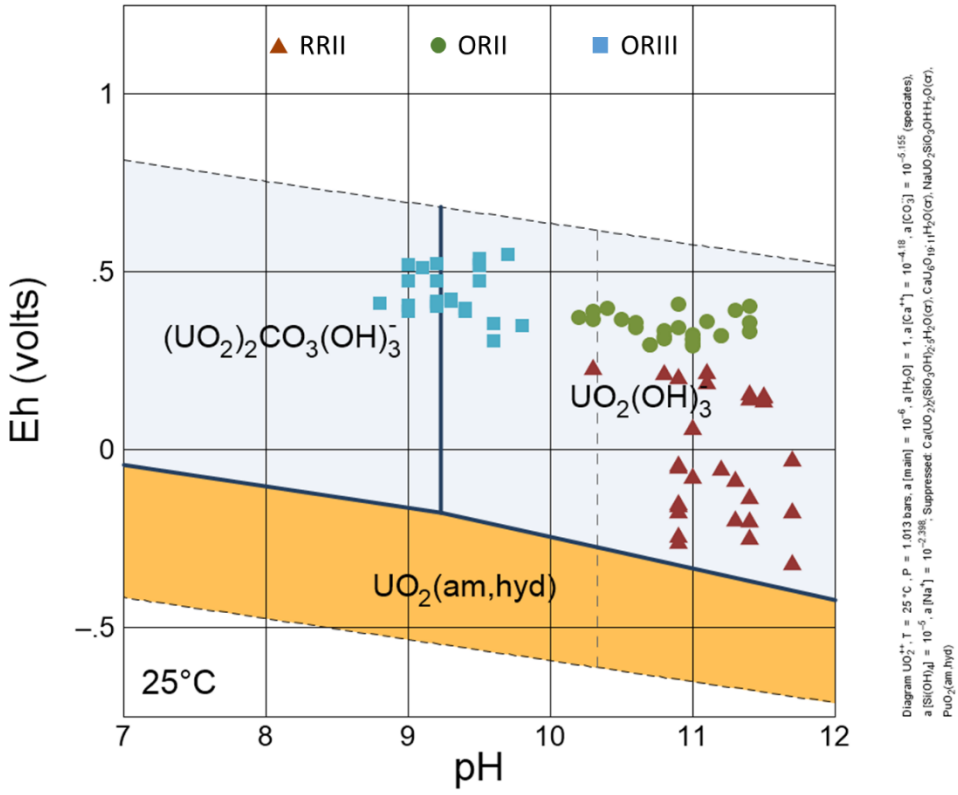

Figure 3: Eh-pH values of samples in SRNL experiments relative to the stability of UO_2(am,hyd) at a uranium activity of 10^{-6} M.

Five mineral phases can adequately explain the uranium concentrations in the SRNL leaching experiments. **Table 7** lists the mineral names and their chemical formulas as they appear in the NEA thermodynamic database. All occur naturally and all are weathering products of uranium associated with nuclear fuel. Shoepite was used as the solubility controlling phase for Oxidized Regions II and III in Denham and Millings (2012), but is too soluble to explain the SRNL experimental results.

Table 7: Minerals and their formulas used to explain SRNL experimental results.

Mineral	Formula in NEA Database
Schoepite	$UO_3{\cdot}2H_2O_{(cr)}$
Becquerelite	$CaU_6O_{19}{\cdot}11H_2O_{(cr)}$
Soddyite	$(UO_2)_2SiO_4{\cdot}2H_2O_{(cr)}$
Na-Boltwoodite	$NaUO_2SiO_3OH{\cdot}H_2O_{(cr)}$
Uranophane	$Ca(UO_2)_2(SiO_3OH)_2{\cdot}5H_2O_{(cr)}$

Figure 4 was constructed using the Oxidized Region II fluid composition reported in King (2018) and shows experimental uranium concentrations versus pH in the Reduced Region II and Oxidized Region II experiments relative to stability fields for four minerals in **Table 7**. The order of solubility of the minerals at pH≅11 is schoepite > becquerelite > uranophane. The white field is aqueous uranium and at ideal solubility control by a mineral, uranium vs. pH values would plot on the lower boundary of that mineral. Values that lie near, but not on, a lower boundary of a mineral stability field may be explained by differences in fluid composition in the experiments compared to those used in calculating the diagram.

For example, the diagram was constructed using the average measured Si concentration of 1 mg/L (3.6E-5 M) and Ca concentration of 1.8 mg/L (4.5E-5 M) reported in Table 3-8 of King (2018) for the Oxidized Region II samples. The carbonate concentration was report by King (2018) as <100 mg/L, and so is calculated here to be 6.5E-5 M, from the measured Ca concentration and the assumption of equilibrium with calcite. A higher silica concentration would shift the uranophane solubility lower. Likewise, the stability fields can shift because of changes in dissolved calcium or sodium concentrations. The nature of the mineral phase can also change the solubility. The thermodynamic data is for crystalline phases. Disordered phases of the same composition would have higher solubilities. Impurities in the crystalline lattice, for example substitutions for calcium or silicon in uranophane, can also increase solubility.

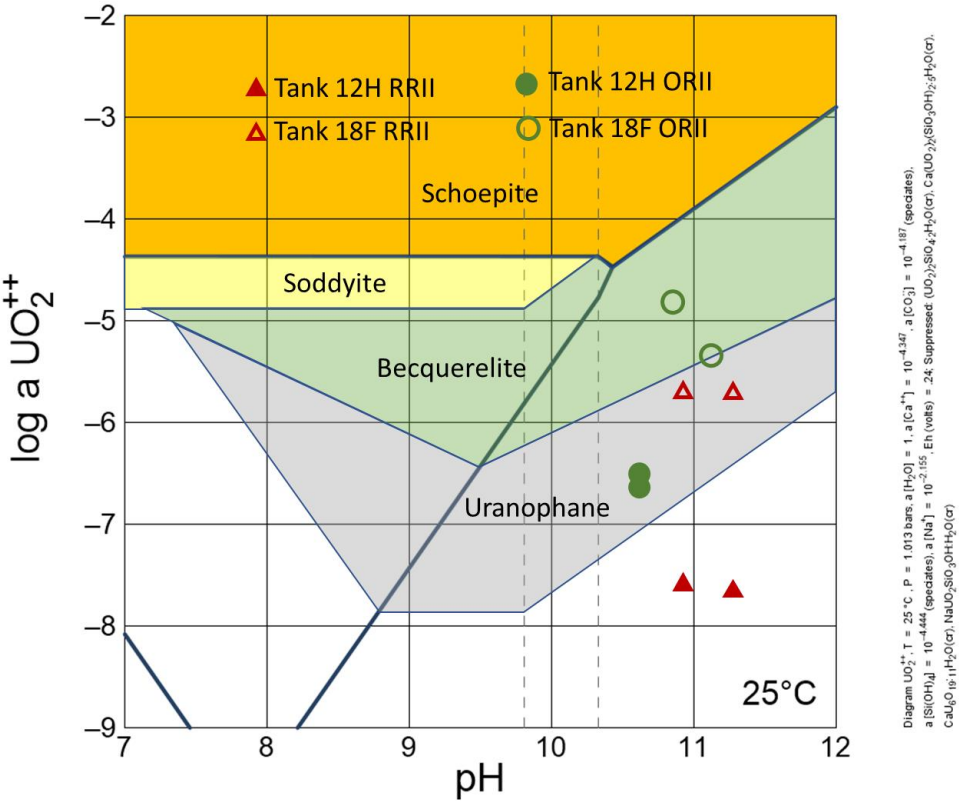

Figure 4: Calculated diagram of uranium concentration vs. pH showing where average sample measurements for the Reduced Region II and Oxidized Region II plot relative to stability fields of five potential solubility controlling minerals.

Higher aqueous concentrations of uranium occurred in the Tank 18F samples across all grout degradation regions. This is the probable result of the different tank cleaning protocols, leaving the Tank 18F samples with a higher mass of soluble uranium. Average uranium concentrations in the Reduced Region II samples and the Oxidized Region IIA sample are explained by becquerelite solubility. The higher average uranium concentration in the Oxidized Region IIB experiment can be explained in multiple ways. It could be the result of the presence of becquerelite and a small amount of schoepite in the initial samples, but not enough schoepite to saturate the solution. This would not be surprising in samples from a tank that was not chemically cleaned and lost 16% of the uranium in the initial wash of

the experimental samples. The higher uranium concentration could also result from impure or poorly crystalline becquerelite.

Na-Boltwoodite or uranophane have nearly the same stability field at the diagram's fluid composition (only uranophane is shown in the figures) and either can explain the uranium leaching from the Region II samples of the Tank 12H experiments. The concentrations and pH values of the Oxidized Region II samples place them slightly above the solubility of Na-Boltwoodite and uranophane. Both Reduced Region II samples plot below the stability fields for Na-Boltwoodite and uranophane. King (2018) did not report a fluid composition for the Reduced Region II experiments, so it is possible it was different enough to expand the stability field of Na-Boltwoodite or uranophane. Fly ash and blast furnace slag were added to one of the Reduced Region II experiments, presumably increasing the silica concentration, and in turn expanding the stability fields of Na-Boltwoodite and uranophane. An approximation of the resulting concentrations of Na^{+}, Ca^{+2}, and $Si(OH)_4$ can be made from modeling of grout degradation and the experiments of Seaman et al. (2020). **Figure 5** shows the expansion of the stability fields for uranophane under conditions derived from these sources. The lower solubilities of Na-Boltwoodite and uranophane can explain the low uranium concentrations in the Reducing Region II experiments on residual waste from Tank 12H, given a fluid composition between that reported by King (2018) for the Oxidized Region II experiments and that resulting from modeling grout degradation.

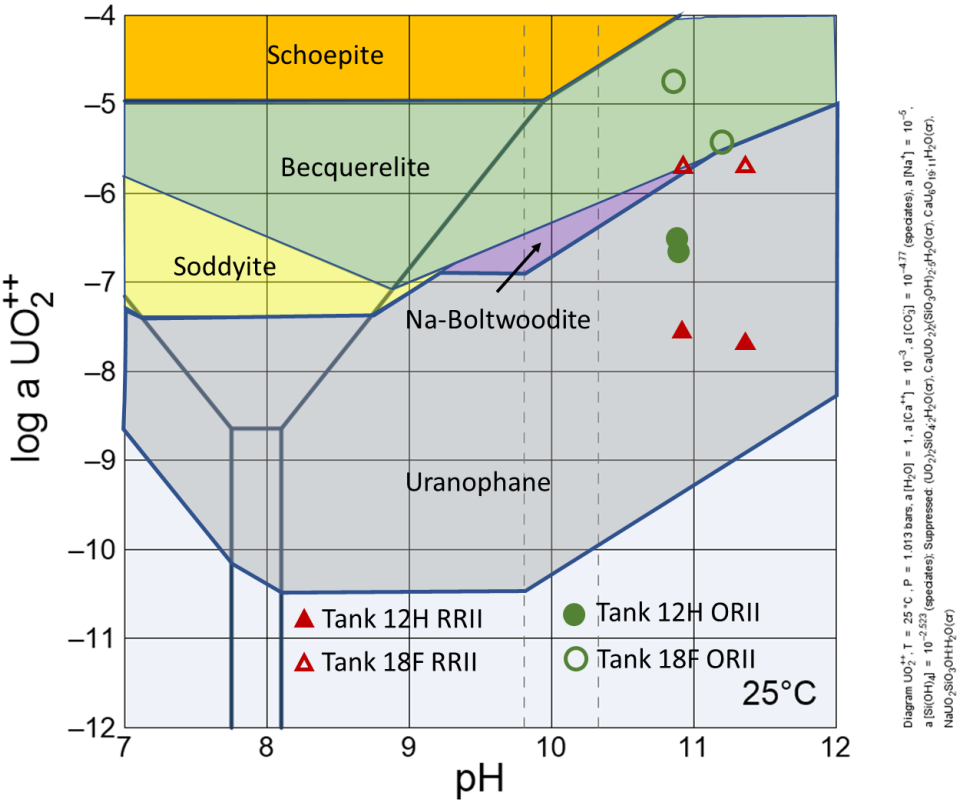

Figure 5: Calculated diagram of uranium concentration vs. pH showing where average sample measurements for Oxidized Region III plot relative to stability fields of four potential solubility controlling mineral at aqueous concentrations of Na^{+}, Ca^{+2}, and $Si(OH)_4$ approximated for addition of cementitious materials.

The minerals used to explain the behavior of uranium in Region II can also explain uranium behavior in Oxidized Region III. **Figure 6** shows uranium activity versus pH and the solubility limits of becquerelite, soddyite, Na-Boltwoodite, and uranophane and the experimental results under Oxidizing Region III conditions. The primary difference from Region II is a significantly higher dissolved inorganic carbon concentration that enhances uranium solubility because of dominant uranium carbonate aqueous complexes. Uranium concentrations in the Tank 18F samples can be explained by solubility of Na-Boltwoodite and uranophane. In one of the Tank 12H experiments the average uranium concentration is below the solubility of uranophane. The reaction vessel broke during this experiment and the solids were exposed to a large volume of high pH solution. The solids were recovered and placed in a new vessel with fresh fluid. King (2018) refers to this sample as highly washed and calculated that 34% of the original uranium mass in the experiment was leached by the wash solution. There are multiple possibilities for the low uranium concentration, including extensive leaching of uranium during exposure to the high pH solution, reactions that caused occlusion of uranium-bearing phases (e.g., silica dissolving and reprecipitating), or a change in the bulk composition of the fluid. King (2018) did not report a solution analysis for this experiment and it is feasible that expansion of the stability fields of Na-Boltwoodite or uranophane by higher aqueous concentrations of Ca^{+2}, Na^{+}, and $Si(OH)_4$ would explain the low uranium concentration.

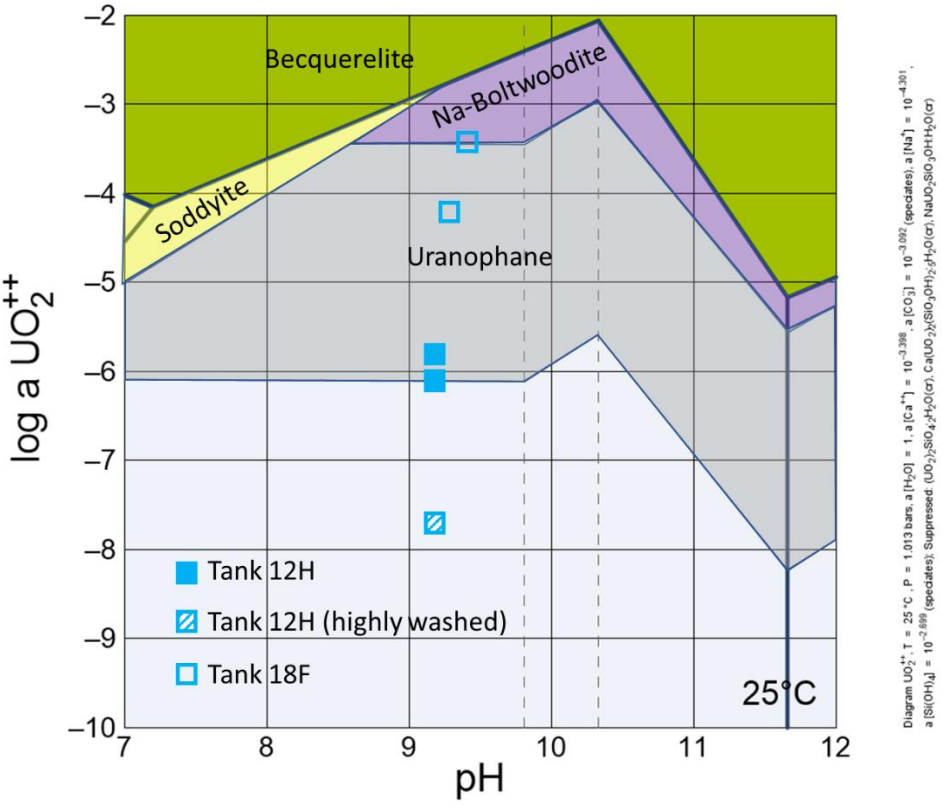

Figure 6: Calculated diagram of uranium concentration vs. pH showing where average sample measurements for the Oxidized Region III experiment plot relative to stability fields of four potential solubility controlling mineral.

The experiments of King and Hobbs (2016 and King (2018) provide excellent information for selecting solid phases for use in predictive models to control leaching of uranium from the residual waste layer. In selecting phases for controlling solubility of uranium in predictive modeling, the future conditions the residual will subjected to must be considered. In particular, the length of time the waste will subjected to these relative to the length of the experiments must be considered. The initial samples for the Tank 18 experiments contained the sodium uranyl carbonate Cejkaite ($Na_4(UO_2)(CO_3)_3$) as identified in King and Hobbs (2016), most of which was likely removed from residual waste in tanks that were chemically cleaned. The initial washing of the experimental samples removed 10-16% of the uranium (not including the special case of the "highly washed" ORIII sample). The remaining uranium was in phases with solubilities similar to becquerelite, Na-Boltwoodite, and uranophane. It is difficult to discern whether reactions occurred during the experiments that altered one mineral to another. Yet, these types of reaction will occur over the timeframes considered in PA modeling.

The initial grout pore fluids in an unbreached tank will have high concentrations of Na^+, Ca^{+2}, and $Si(OH)_4$, favoring formation of Na-Boltwoodite and uranophane. After the tank breaches, the Ca/Na ratio in the pore waters will increase as infiltration rapidly leaches sodium from the grout. Uranophane then becomes the thermodynamically favored mineral. Interestingly, Wellman (2008) found uranyl phosphates to be the most stable phase in concrete wasteforms, forming after uranophane. However, little is known yet about the prevalence of phosphate in SRS tank grout and uranyl phosphate mineral are not considered here. Multiple investigators have observed the general sequence of minerals in U-Ca-Si-H_2O systems prevalent in concrete wasteforms (Golovich et al., 2011):

$$\text{Schoepite} \rightarrow \text{Becquerelite} \rightarrow \text{Uranophane}$$

Golovich et al. (2014) describe experiments in which concrete was spiked with uranium solutions. In 10^{-3} M solutions, a hydroxide phase resembling schoepite initially forms, then reacts to form an apparent mixed phase of becquerelite and uranophane. More concentrated uranium spikes resulted in uranophane formation.

It is recommended here that both becquerelite and uranophane be considered as solubility limiting phases for uranium in updated PA models. Becquerelite would be a "pessimistic" choice because of its higher solubility, whereas uranophane would be optimistic and defensible based on the SRNL leaching experiments and literature studies. There is no evidence from the SRNL leaching studies that uranium would be coprecipitated. **Table 8** shows the calculated solubilities becquerelite and uranophane using the updated NEA data and fluid compositions of Denham and Millings (2012). Note that these solubilities are different than those shown in Figures 3 and 5 because the diagrams were calculated using the SRNL experimental fluid compositions. The solubilities are given for only Oxidized Region II and Oxidized Region III, using the assumption that conditions in tank grout will not be sufficiently reducing to convert U(VI) to U(IV). If PA modeling assumes otherwise, then UO_2(am,hyd) should be used to limit solubility to that listed in Table 3 above. The solubilities in Table 8 will need to be recalculated if updated grout modeling changes fluid compositions in the oxidized regions from that assumed in Denham and Millings (2012).

Table 8: Solubilities of becquerelite and uranophane calculated for Oxidizing Region II and Oxidizing Region III using updated NEA thermodynamic data and fluid compositions assumed in Denham and Millings (2012).

Mineral	Oxidized Region II	Oxidized Region III
Becquerelite	3E-6 M	9E-7 M
Uranophane	2E-7 M	1E-7 M

Neptunium

The results of neptunium leaching from residual waste are more difficult to interpret than leaching of other radionuclides because most of the concentrations were below detection limits. The neptunium concentrations in Oxidized Region III experiments were above detection limits and higher than the concentrations in the other experiments. Detection limits and concentrations above detection limits were generally higher in the Tank 18F experiments than the Tank 12H experiments. The neptunium concentrations in the SRNL leaching experiments were orders of magnitude lower than the solubility controls calculated in Denham and Millings (2012) for discrete neptunium phases. Coprecipitation with iron minerals does not explain the low concentrations because the concentrations in the Oxidized Region III experiments are too high and the lower concentrations at pH≅11 do not conform to the pattern of iron mineral solubility versus pH.

Several investigators have studied and confirmed coprecipitation of neptunium in uranophane (Buck et al., 2003; Burns et al., 2004; Klingensmith and Burns, 2007; Murphy and Grambow, 2008; Goana et al., 2013). Burns et al. (2004) synthesized uranophanes with 29- 182 ppm neptunium (as Np/(Np+U)). At these concentrations, neptunium coprecipitated in uranophane could control neptunium concentrations in solution to 4-5 orders of magnitude lower than uranium concentration. Given the average experimental concentrations of uranium, 2.5E-7 at pH=10.6 and 1.5E-6 at pH=9.2, a uranophane with 100 ppm Np would yield dissolved neptunium concentrations approximately 4 orders of magnitude below the uranium concentrations. The neptunium concentrations observed were approximately an order of magnitude higher. Nevertheless, this is a possible mechanism for the control of neptunium release from residual waste, but cannot be recommended without additional experimental data. Heberling et al. (2008) coprecipitated neptunium(V) in calcite at neptunium concentrations of 1900-5100 ppm as a rind on seed crystals. However, the solubility of calcite is too high for coprecipitated neptunium to account for the low neptunium concentrations observed in the SRNL leaching experiments.

Murphy and Grambow (2008) derived a $\log K_{sp}$ for a uranophane-like mineral with Np(V) substituted for U(VI) from the data of Burns et al. (2004) to describe the thermodynamics of Np(V) coprecipitation in uranophane. **Figure 7** shows a stability field of Np-uranophane calculated using the derived K_{sp} and a silica concentration of 0.001 M. It explains the SRNL leaching data well, yet cannot be recommended as a solubility control in PA modeling because of the uncertainty in the thermodynamic data.

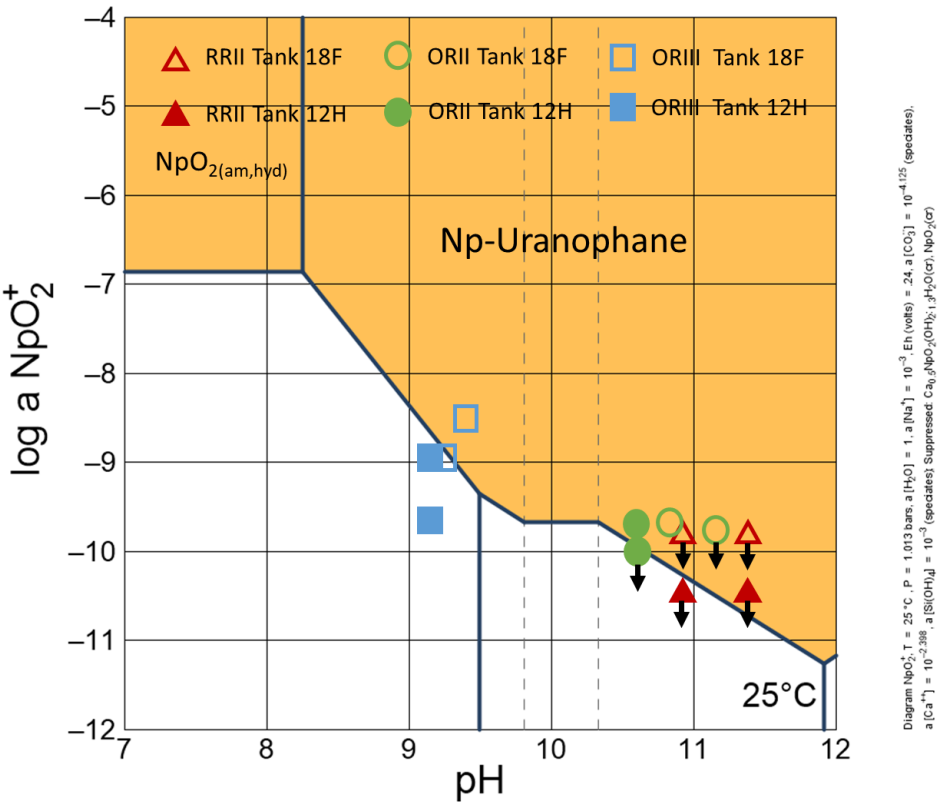

Figure 7: Hypothetical stability field for a uranophane-like Np(V) phase calculated using a logKsp derived by Murphy and Grambow (2008); arrows indicate concentrations below detection limits.

Finally, it is possible that solubility of neptunium is controlled by a partially crystallized NpO_2 phase. **Figure 8** (following page) shows the solubility of crystalline $NpO_{2(cr)}$ compared to the solubility of $NpO_{2(am,hyd)}$. The neptunium concentrations measured in the SRNL leaching experiments would fall between $NpO_{2(am,hyd)}$/$Ca_{0.5}NpO_2(OH)_2 \cdot 1.3H_2O$ and crystalline $NpO_{2(cr)}$. However, this cannot be used as a solubility control without a rigorous way to derive the $logK_{sp}$ of a partially crystalline NpO_2 phase and it would not explain the higher concentrations associated with the Oxidized Region III experiments.

With the lack of any rigorous explanation for the neptunium concentrations, it is recommended here that the calculated solubilities for $NpO_{2(am,hyd)}$ and $Ca_{0.5}NpO_2(OH)_2 \cdot 1.3H_2O$ be used as a "worst case" in PA modeling. The average of the experimental Oxidized Region III concentrations could be used for that grout degradation stage and the highest detection limits could be used for the other stages.

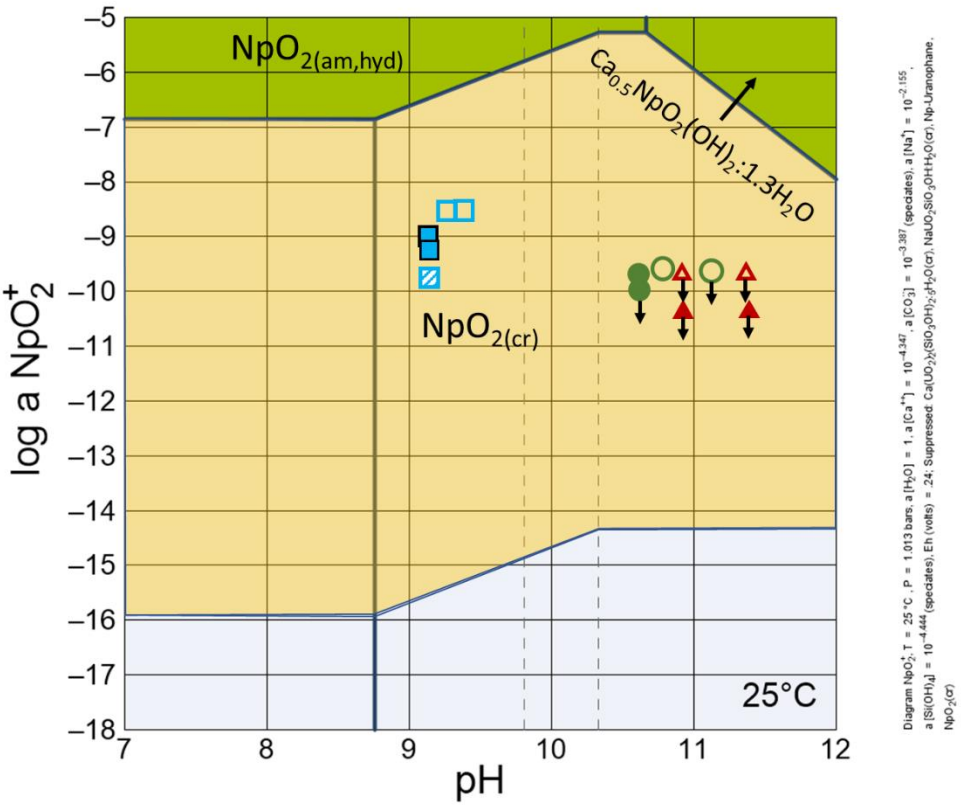

Figure 8: Stability field of crystalline $NpO_{2(cr)}$ compared to other neptunium phases; arrows indicate concentrations below detection limits.

Plutonium

Plutonium concentrations in the SRNL experiments range from $<10^{-13}$ to 10^{-8} M, with all concentrations $>10^{-10}$ occurring in the Tank 18F experiments. It is important that the concentrations of plutonium in Tank 18F experiments are generally higher than those in Tank 12H experiments. A major difference between the two tank samples is that Tank 12H was chemically cleaned and Tank 18F was not. That suggests the possibility of a moderately soluble solid phase occurring in the Tank 18F samples that was dissolved out of the Tank 12H samples by chemical cleaning.

Hobbs (2012) discussed the possibility of Pu(IV)-carbonate occurring in the residual waste as a result of high dissolved carbonate concentrations in tank liquids. If a Pu(IV)-carbonate existed in the waste before cleaning, it would be completely dissolved by chemical cleaning with oxalic acid. Thus, it might exist in the Tank 18F residual waste, but not in the Tank 12H residual waste. Nevertheless, a Pu(IV)-carbonate phase cannot explain the leaching data in the SRNL experiments. The stability field for $PuOCO_3 \cdot H_2O$ in a solution in equilibrium with atmospheric carbon dioxide is shown in **Figure 9** (following page) using thermodynamic data from Yamguchi et al. (1994). They give the log K_{sp} value for this phase as <48 for the reaction:

$$PuOCO_3 \cdot xH_2O = Pu^{+4} + 2OH^- + CO_3^{-2} + (x-1)H_2O$$

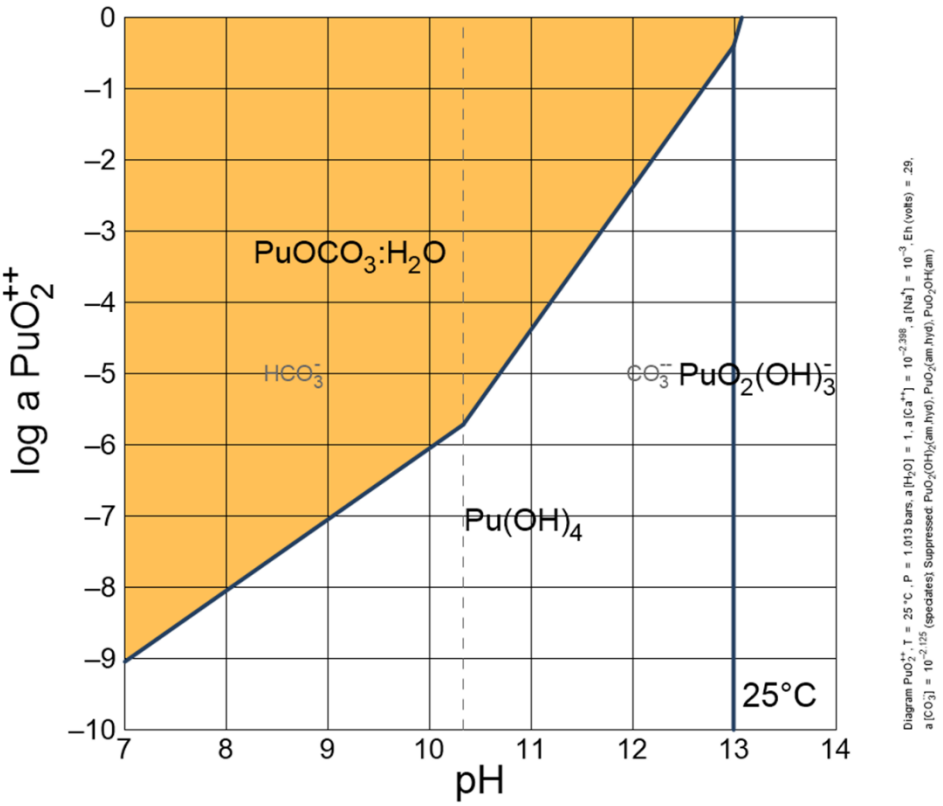

Figure 9: Stability field of a Pu(IV) in equilibrium with atmospheric CO_2, calculated using thermodynamic data from Yamaguchi et al (1994).

Adjusting the $\log K_{sp}$ to lower values could yield a solubility of 1E-8 M at pH=9, or using an even lower value at pH=11. However, as the $\log K_{sp}$ decreases, the boundaries of the stability field expand in parallel. Hence, the solubility is always 2.7 orders of magnitude higher at pH=11 than at pH=9. This difference in solubilities was not observed in the SRNL experiments at Oxidized Region II (pH≅11) and Oxidized Region III (pH≅9).

A better explanation is provided by the work of Neck et al. (2007a and 2007b), who discuss apparent higher solubility of colloidal $PuO_{2(am,hyd)}$ particles than coagulated masses of $PuO_{2(am,hyd)}$. In experiments on solubility of amorphous hydrated PuO_2 ($PuO_{2(am,hyd)}$), they compared samples that were subjected to ultrafiltration to those that were not. At pH>9 the ultrafiltered samples had solubilities very close to those calculated using NEA thermodynamic data. The unfiltered samples had higher plutonium concentrations, averaging about $10^{-8.3}$ M. Neck et al (2007a) concluded that that the particle diameters were on the order of 1.5-2.0 nm, able to pass through the 0.1 um filters used in sampling the SRNL experiments. **Figure 10** (following page) shows the average concentrations for each SRNL experiment relative to the calculated solubility of $PuO_{2(am,hyd)}$ and the solubility including colloidal particles. The data from the Tank 12H experiments is explained by the solubility of $PuO_{2(am,hyd)}$ with no colloidal particles.

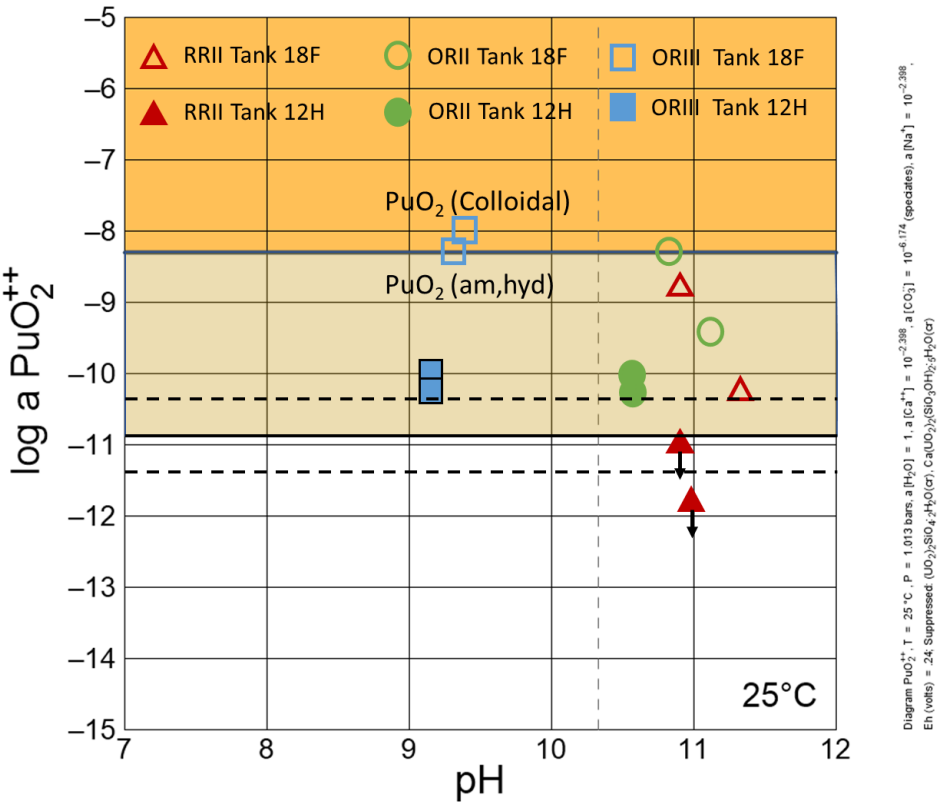

Figure 10: Plutonium leachability data from SRNL experiments compared to calculated solubility of PuO2(am,hyd) with no colloidal particles (dashed lines show thermodynamic uncertainty given by Grenthe et al. (2020)) and with colloidal particles after Neck et al. (2007a).

It is reasonable that the different tank cleaning regimes resulted in the presence or absence of colloidal particles. The mechanical cleaning of Tank 18F may have created colloidal particles with the agitation of the waste or by precipitation in water remaining after cleaning. Cleaning of Tank 12H with oxalic acid would have dissolved any existing colloidal particles and left fresh surfaces of coagulated $PuO_{2(am,hyd)}$. It is likely the lower plutonium concentrations in the Tank 12H experiments reflect the lack of colloidal particles.

For PA modeling it is recommended that the updated value for the calculated solubility of $PuO_{2(am,hyd)}$ – 2E-11M -- be used to account for leachability of plutonium isotopes. Sensitivity analyses can be run using the colloid inclusive solubility of $10^{-8.3}$ M.

Iodine

Denham and Millings (2012) recommended using no solubility controls to model leaching of I-129 from waste tanks. I-129 was only analyzed in the Tank 12H experiments and concentrations were all below detection limits that ranged from 10^{-7} to 19^{-8} M. As mentioned in Layton (2018), I-129 may be controlled by precipitation of low solubility metal iodides such as AgI and HgI_2. The solubilities of iodine in these, or other metal iodides, depend on the concentration of the metal. Both silver and mercury are redox sensitive and iodide salts of these metals do not occur at low Eh values. **Figure 11** (following page) is an Eh-pH diagram of the silver and iodine system. The conversion of AgI to Ag-metal varies with iodide

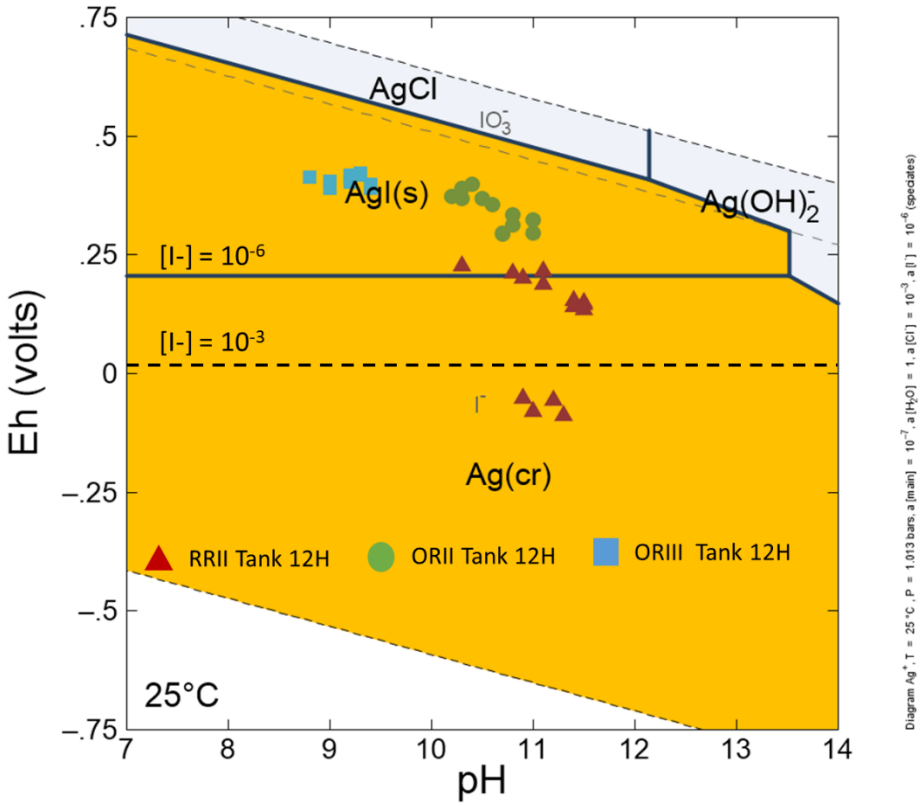

Figure 11: Eh-pH diagram for silver-iodine system, showing stability fields for AgI(s) and Ag metal and Eh-pH measurements from Tank 12H experiments.

concentration. At an iodide concentration of 10^{-6}M, most of the Reducing Region II measurements are below the stability of AgI suggesting there should be no solubility control for those. Yet, the I-129 concentrations are below detection limits.

Figure 12 (following page) shows the stability fields for mercury solid phases in the mercury-iodine system. All of the Reducing Region III samples plot in the elemental mercury field. The Oxidized Region II samples plot in the field for the aqueous complex $Hg(OH)_2$. Only samples from the Oxidized Region III experiments plot within a stability field of a phase that could control iodine solubility.

The stability fields do vary with composition, for example with silver concentration. There are also many other metals in tank waste that could control solubility of iodine. It is also quite possible that I-129 is coprecipitated with in a phase in which iodine is not a dominant component. For example, iodate (IO3-) is known to coprecipitate with calcite (Zhang et al., 2013; Katsenovich et al, 2020).

In the absence of clarity on a mechanism controlling I-129 concentrations in the SRNL experiments, it is recommended that the highest detection limits be used in PA modeling with the caveat that the low leachability is based on two leaching experiments. Sensitivity analyses should be performed using no solubility controls.

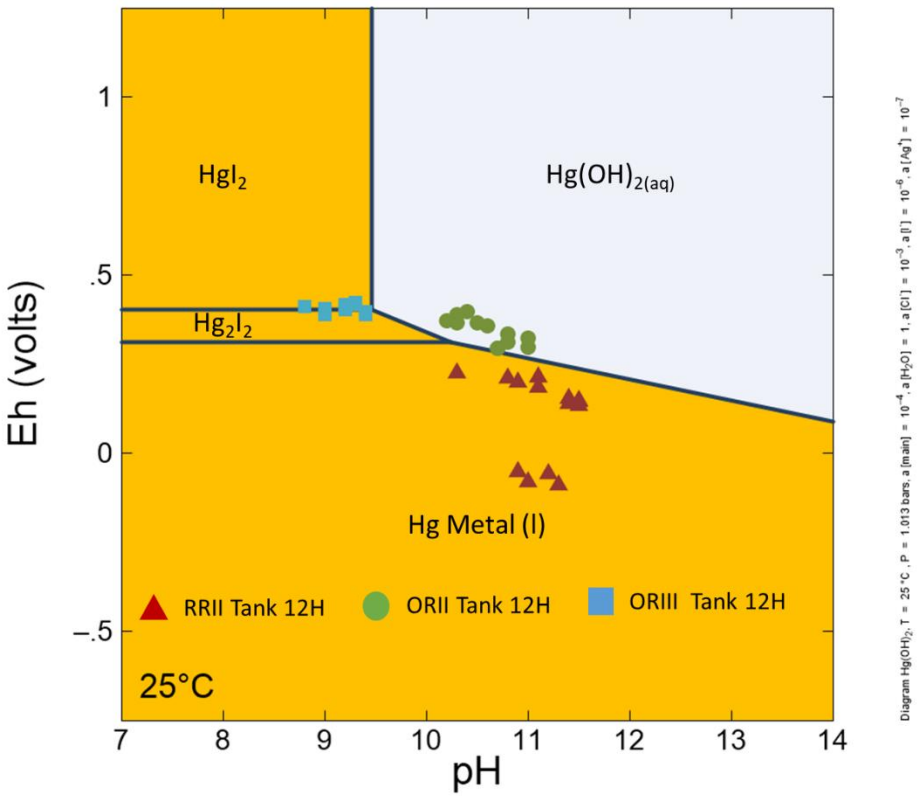

Figure 12: Eh-pH diagram for the mercury-iodine system showing stability fields for mercury iodide phases, mercury metal and Eh-pH measurements from Tank 12H experiments.

One interesting observation about the measured Eh-pH values is their proximity (except for 4 values) to redox boundaries. King (2018) reported 9 wt.% mercury in the Tank 12H residual waste. So, it is feasible that mercury redox chemistry is controlling the Eh measurements and may be a significant redox buffer within the system. Minimal kinetic hindrance to transfer of electrons within the mercury redox system (hence, their use in calomel electrodes) and the mass of mercury in the residual waste may explain the difficulties encountered in the SRNL experiments when trying to produce the extreme redox conditions predicted by the model of Denham and Millings (2012). If that is the case, it follows that mercury would tend to poise the Eh in the residual waste layer of a closed tank.

Conclusion

Experimental radionuclide leachability from residual waste samples from two SRS high level waste tanks (King and Hobbs, 2016; King, 2018) provide insights and guidance on selecting solubility controls for modeling release of radionuclides from closed waste tanks. The goal of the experiments was to leach residual waste samples under conditions similar to those predicted for various stages of closed tank aging. The results of these experiments were interpreted here within the framework of the conceptual model developed by Denham and Millings (2012) and recommendations on controlling release of Tc-99, uranium, Np-237, plutonium, and I-129 were updated.

The following observations and recommendations were made in this document:

- Tc-99 concentrations in experimental leachate were low for all conditions in samples from both Tanks 18F and 12H. The reasons are poorly understood and may be as simple as a limited mass of Tc-99 available for leaching. Coprecipitation in iron or aluminum phases is not the sole controlling factor for Tc-99 because leachate concentrations are too high and do not vary with different stages of grout degradation. Other potential controls on leachability are transitory and likely not operable in closed tank conditions. Therefore, it is recommended that leaching be modeled by dissolution of $TcO_{2(am,hyd)}$ for Reducing Region II and with no solubility control for oxidizing conditions. If new grout degradation modeling results in an Eh value greater than -200 mV for Reducing Region II, then no solubility controls should be used to limit Tc-99 leachability.
- The SRNL experiments did not achieve conditions reducing enough for uranium to exist as $UO_{2(am,hyd)}$. This may also be true of future modeling, if guided by experimental evidence. In this case, solubility of becquerelite and uranophane can explain the leachability of uranium, with becquerelite being a pessimistic choice. The corresponding solubilities are shown below.

Mineral	Oxidized Region II	Oxidized Region III
Becquerelite	3E-6 M	9E-7 M
Uranophane	2E-7 M	1E-7 M

- It is likely that leachability of Np-237 is solubility controlled and future work on neptunium silicates may provide more defensible controls than presented here. In light of the speculative nature of the mineralogic controls, it is recommended that the experimental results be used to control leachability, but that calculated solubilities for $NpO_{2(am,hyd)}$ and $Ca_{0.5}NpO_2(OH)_2 \cdot 1.3H_2O$ be applied in “worst case” sensitivity studies.
- Plutonium leachability in the Tank 12H experiments conform to the previously used solubility control by $PuO_{2(am,hyd)}$ with an updated solubility of 2E-11 M for all conditions. It is likely that the higher leachability of plutonium in the Tank 18F experiments reflects the presence of colloidal plutonium particles that remained in the absence of chemical cleaning of the tank.
- I-129 concentrations in the SRNL leachability experiments are all below detection limits. This could be caused by precipitation of multiple metal iodides or coprecipitation with a moderately soluble phase. This cannot be discerned because there are no detectable concentrations. Therefore, it is recommended that the highest detection limits be used to control solubility of I-129 in future PA modeling, with a discussion of the caveat that this is based on only two samples. Sensitivity studies with no solubility controls should be done for comparison.

References

Bethke, C.M., B. Farrell, and M. Sharifi, 2021. The Geochemist's Workbench®, Release 15, GWB Reaction Modeling Guide. Aqueous Solutions, LLC, Champaign, Illinois.

Boglaienko, D. and T. Levitskaia, 2019. The abiotic reductive removal and subsequent incorporation of Tc(IV) in iron oxides: a frontier review. *Environmental Science: Nano*, 6, 3492-3500.

Buck, E.C., B.K. McNamara, M. Douglas and B.D. Hanson, 2003. Possible Incorporation of Neptunium in Uranyl (VI) Alteration Phases, PNNL-14277, Pacific Northwest National Laboratory, Richland, WA.

Burns, P.C., K.M. Deely, and S. Skanthakumar, 2004. Neptunium incorporation into uranyl compounds that form as alteration products of spent nuclear fuel: Implications for geologic repository performance. *Radiochimica Acta,* 92, 3.

Denham, M.E. and M.R. Millings, 2012. Evolution of chemical conditions and estimated solubility controls on radionuclides in the residual waste layer during post-closure aging of high level waste tanks. SRNL-STI-2012-00404, Savannah River National Laboratory, Aiken, SC.

Frederickson, J.K., J.M. Zachara, A.E. Plymale, S.M. Heald, J.P. McKinley, D.W. Kennedy, C. Liu and P. Nachimuthu, 2009. Oxidative dissolution potential of biogenic and abiogenic TcO_2 in subsurface sediments, *Geochimica et Cosmochimica Acta*, 73(2009), 2299-2313.

Gaona, X., E. Wieland, J. Tits, A.C. Scheinost and R. Daehn, 2013. Np(V/VI) redox chemistry in cementitious systems: XAFS investigations on the speciation under anoxic and oxidizing conditions, *Applied Geochemistry*, 28 (2013), 109-118.

Golovich, E.C., D.M. Wellman, R.J. Serne and C.C. Bovaird, 2011. Summary of Uranium Solubility Studies in Concrete Waste Forms and Vadose Zone Environments, PNNL-20726, Pacific Northwest National Laboratory, Richland, WA.

Golovich, E.C., S.V. Mattigod, M.M.V. Snyder, L.J. Powers, G.A. Whyatt and D.M. Wellman, 2014. Radionuclide Migration through Sediment and Concrete: 16 Years of Investigations, PNNL-23841, Pacific Northwest National Laboratory, Richland, WA.

Grenthe, I., J. Fuger, R.J.M. Konings, R.J. Lemire, A.B. Muller, C.N-T. Cregu, and H, Wanner, 1992. Chemical thermodynamics of uranium. North-Holland, Amsterdam.

Grenthe, I., X. Gaona, A.V. Plyasunov, L. Rao, W.H. Runde, B. Grambow, R.J.M. Konings, A.L. Smith, E.E. Moore, 2020. Second update on the chemical thermodynamics of uranium, neptunium, plutonium, americium, and technetium. North-Holland, Amsterdam.

Guillaumont, R.T., T. Fanghänel, J.Fuger, I. Grenthe, V. Neck, D.A. Palmer, M.H. Rand, 2003. Update on chemical thermodynamics of uranium, neptunium, plutonium, americium, and technetium. Nuclear energy Agency, Organisation for Economic Co-operation and Development, Elsevier, Amsterdam.

Heberling, F., M.A. Denecke and D. Bosbach, 2008. Neptunium (V) coprecipitation with calcite, *Environmental Science & Technology* 42(2), 471-476.

Hobbs, D.T., 2012. Form and aging of plutonium in Savannah River Site waste tank 18. SRNL-STI-2012-00106. Savannah River National Laboratory, Aiken, SC.

Katsenovich, Y., R.T.Gort, X. Lugo, R. Gudavalli, N.P. Qafoku, V. Freedman, L. Lagos, 2020. Iodine co-precipitation with calcium carbonate in the presence of silica ions. Conference Paper 20360, Waste Management 2020 Conference, Phoenix AZ

King, W.D. and D.T. Hobbs, 2016. Determining the release of radionuclides from Tank 18F waste residual solids: FY2016 Report. SRNL-STI-2016-00432, Revision 0. Savannah River National Laboratory, Aiken, SC.

King, W.D., 2018. Determining the release of radionuclides from SRS Tank 12H waste residual solids following tank closure. SRNL-STI-2018-00484, Revision 1. Savannah River National Laboratory, Aiken, SC.

Klingensmith, A.L., and P.C. Burns, 2007. Neptunium substitution in synthetic uranophane and soddyite. *American Mineralogist,* 92, 1946-1951.

Layton, M.H., 2018a. Evaluation of waste release testing results against the tank farm performance assessment waste release model. SRR-CWDA-2016-00086, Revision 1. Savannah River Remediation, LLC, Aiken, SC.

Layton, M.H., 2018b. Waste tank residuals properties. N-ESR-H-00040, Revision 2. Savannah River Remediation, LLC, Aiken, SC.

Lemire, R.J., J. Fuger, H. Nitsche, P. Potter, M.H. Rand, J. Rydberg, K. Spahui, J.C. Sullivan, W.J. Ullman, P. Vitorge, and H. Wanner, 2001. Chemical thermodynamics of neptunium and plutonium. North-Holland, Amsterdam.

Meena, A. and Y. Arai, 2017.. Environmental geochemistry of technetium. *Environmental Chemistry Letters*, 15, 241-263.

Murphy, W.M. and B. Grambow, 2008. Thermodynamic interpretation of neptunium coprecipitation in uranophane for application to the Yucca Mountain repository, *Radiochimica Acta*, 96(2008), 563-567.

Neck, V., A. Marcus and T. Fanghänel, 2007. Solubility of plutonium hydroxides/hydrous oxides under reducing conditions and in the presence of oxygen, *Comptus Chimie,* 10(2007), 959-977.

Neck, V., M. Altmaier, A. Seibert, J.I. Yun, C.M. Marquardt and T. Fanghänel, 2007. Solubility and redox reactions of Pu(IV) hydrous oxide: Evidence for the formation of PuO2+x(s, hyd), *Radiochimica Acta,* 95(2007), 193-207.

Peretyazhko, T., J.M. Zachara, S.M. Heald, B.-H. Jeon, R. K. Kukkadapu, C. Liu, D. Moore and C.T. Resch, 2009. Heterogeneous reduction of Tc(VII) by Fe(II) at the solid–water interface, *Geochimica et Cosmochimica Acta* 72(2009), 1521-1539.

Poirier, M.R., F.F. Fondeur, D.M. Missimer, M.E. Summer and S.D. Fink, 2010. Analysis of Solids Remaining Following Chemical Cleaning in Tank 6F, SRNL-STI-2009-00816, Rev.0, Savannah River National Laboratory, Aiken, SC.

Rard, J.A., M.H. Rand, G. Anderegg, and H. Wanner, 1999. Chemical thermodynamics of technetium. North-Holland, Amsterdam.

Seaman, J.C., S.P. Simner, and C. Logan, 2020. Aqueous and solid phase characterization of potential tank fill materials. SREL Doc.: R-21-0001, Savannah River Ecology Laboratory, The University of Georgia, Aiken, SC.

Szecsody, J.E., D.P. Jansik, J.P. McKinley and N.J. Hess, 2014. Influence of alkaline co-contaminants on technetium mobility in vadose zone sediments, *Journal of Environmental Radioactivity* 135(2014), 147-160.

Wellman D.M., K.E. Parker, C.C. Bovaird, R.M. Ermi, S.V. Mattigod and M.I. Wood, 2008. Effect of Concrete Waste Form Properties on Radionuclide Migration, PNNL-17808, Pacific Northwest National Laboratory, Richland, WA.

Yamaguchi, T., Y. Sakamoto, and T. Ohnuki. Effect of the Complexation on Solubility of Pu(IV) in Aqueous Carbonate System. *Radiochimica Acta*, 66/67, 9-14.

Zachara, J.M., S.M. Heald, B.-H. Jeon, R.K. Kukkadapu, C. Liu, J.P. McKinley, A.C. Dohnalkova and D.A. Moore, 2007. Reduction of pertechnetate [Tc(VII)] by aqueous Fe(II) and the nature of solid phase redox products, *Geochimica et Cosmochimica Acta,* 71(2007), 2137-2157.

Zhang, S., C. Xu, D. Creeley, Y-F. Ho, H-P. Li, R. Grandbois, K.A. Schwehr, D.I. Kaplan, C.M. Yeager, D. Wellman, and P. Santschi, 2013. Iodine-129 and Iodine-127 speciation in groundwater at the Hanford Site, U,S.: Iodate incorporation in calcite. *Environmental Science & Technology*, 47, 9635-9642.

Appendix 1: Results from residual waste leaching experiments done by King and Hobbs (2016) and King (2018)

Tank 18F Average Values (King and Hobbs, 2016)

Measured pH, E_h, and Metal Concentrations for Each Pore Water Test Condition Using Actual Tank 18F Residual Solids.

Test Condition	Sample ID	Additives	Atmosphere	E_h[a] (mV)	pH[a]	Pu[a] (M)	U[a,d] (M)	Tc[a] (M)	Np[b] (M)
RRII	E	$Ca(OH)_2$, $CaCO_3$, FeS	continuous N_2 purge	-208	10.9	2E-9	2E-6	<6E-10	<2E-10
RRII	F	CFS[c], FeS	continuous N_2 purge	-196	11.4	7E-11	2E-6	<6E-10	<2E-10
ORII	A	$Ca(OH)_2$, $CaCO_3$	continuous air purge	+351	11.2	4E-10	4E-6	1E-8	<2E-10
ORII	B	$Ca(OH)_2$, $CaCO_3$	continuous air purge	+328	10.8	6E-9	2E-5	1E-8	3E-10
ORIII	C	$CaCO_3$	continuous air or CO_2-stripped air purge	+520	9.4	1E-8	4E-4	1E-8	4E-9
ORIII	D	$CaCO_3$	continuous air or CO_2-stripped air purge	+493	9.3	6E-9	7E-5	6E-9	1E-9

[a] average data from final 4 weeks
[b] average data from final 2-3 weeks
[c] CFS = cement, flyash, and slag grout solids
[d] due to nearly complete U dissolution observed during washing these leachate concentrations are likely well below solubility limits

Tank 12H Average Values (King, 2018)

Measured pH, E_h, and Metal Concentrations for Each Condition Using Tank 12H Residual Solids.

Test Condition	Sample ID	Additives	Atmosphere/ Condition	E_h (mV)	pH	Molarity				
						Pu[a]	U[a]	Tc[a]	Np[a]	I[a]
RRII	A	$Ca(OH)_2$, $CaCO_3$, FeS	continuous N_2 purge; unwashed	+205[b]	10.8[b]	≤2E-11[b]	4E-8[b]	3E-9[b]	≤5E-11[b]	<5E-7[b]
	B	CFS[c], FeS		+145[b]	11.5[b]	≤1E-11[b]	3E-8[b]	1E-8[b]	<5E-11[b]	<2E-7[b]
	A	$Ca(OH)_2$, $CaCO_3$, FeS	continuous N_2 purge; washed	-64[d]	11.0[d]	≤3E-12[d]	9E-9[d]	≤6E-10[d]	<5E-11[d]	<3E-7[d]
	B	CFS[c], FeS		-71[d]	11.3[d]	<1E-12[d]	1E-8[d]	2E-9[d]	<5E-11[d]	<1E-7[d]
ORII	A	$Ca(OH)_2$, $CaCO_3$	continuous air purge; washed	+340[e]	10.6[e]	1E-10[e]	3E-7[e]	1E-8[e]	2E-10[e]	≤3E-8[e]
	B	$Ca(OH)_2$, $CaCO_3$		+341[e]	10.6[e]	9E-11[e]	2E-7[e]	8E-9[e]	≤1E-10[e]	<1E-7[e]
ORIII	A	$CaCO_3$	continuous air or CO_2-stripped air purge; washed	+404[e]	9.2[e]	1E-10[e]	1E-6[e]	6E-9[e]	9E-10[e]	<1E-7[e]
	B	$CaCO_3$		+406[b]	9.2[b]	1E-10[b]	2E-6[b]	6E-9[b]	1E-9[b]	≤1E-7[b]
	B	$CaCO_3$	continuous air or CO_2-stripped air purge; highly washed	+410[f]	9.2[f]	6E-11[f]	2E-8[f]	≤2E-10[f]	2E-10[f]	<1E-7[f]

[a] isotopes: Pu-238/-239/-240; U-235/-238; Tc-99; Np-237; I-129
[b] average data from first 4 weeks
[c] CFS = cement, flyash, and slag grout solids
[d] average data from final 2 weeks
[e] 8-week average
[f] average data from final 4 weeks